Received Date : 14-Jul-2019

Revised Date : 06-Sep-2019

Accepted Date : 25-Oct-2019

Title:

Structural conformation and self-assembly process of p31-43 gliadin peptide in aqueous solution. Implications for celiac disease.

Authors:

María Georgina Herrera[1#], María Florencia Gómez Castro[2#], Eduardo Prieto[3], Exequiel Barrera[4], Verónica I. Dodero[5], Sergio Pantano[4,6], and Fernando Chirdo[2].

# these authors equally contributed to this work

Institutions:

1. Instituto de Química y Fisicoquímica Biológicas - IQUIFIB (UBA-CONICET), Argentina.
2. Instituto de Estudios Inmunológicos y Fisiopatológicos (IIFP, UNLP-CONICET), Argentina.
3. Instituto de Investigaciones Fisicoquímicas Teóricas y Aplicadas (INIFTA, UNLP-CONICET), Argentina.
4. Institut Pasteur de Montevideo, Uruguay.
5. Bielefeld University, Faculty of Chemistry, Germany.
6. Shanghai Institute for Advanced Immunochemical Studies, ShanghaiTech University, Shanghai, China.

Corresponding author: Fernando Chirdo. fchirdo@gmail.com

Running title: Characterization of the self-organized of p31-43 gliadin peptide.

Article type : Original Article

Abbreviations. CeD, Celiac Disease; BODIPY, boron-dipyrromethene; CD, Circular Dichroism; PPII, poly-proline II; AFM, Atomic Force Microscopy; DLS, Dynamic Light Scattering, MD, Molecular Dynamics Simulation.

Keywords: celiac disease, gliadin p31-43 peptide, secondary structure, oligomers, self-assembly.

Abstract

Celiac Disease (CeD) is a highly prevalent chronic immune-mediated enteropathy developed in genetically predisposed individuals after ingestion of a group of wheat proteins (called gliadins and glutenins). The 13mer α-gliadin peptide, p31-43, induces proinflammatory responses, observed by *in vitro assays* and animal models, that may contribute to innate immune mechanisms of CeD pathogenesis. Since a cellular receptor for p31-43 has not been identified, this raises the question of whether this peptide could mediate different biological effects. In this work, we aimed to characterize the p31-43 secondary structure by different biophysical and *in silico* techniques. By Dynamic Light Scattering (DLS) and using an oligomer/fibril-sensitive fluorescent probe, we showed the presence of oligomers of this peptide in solution. Furthermore, Atomic Force Microscopy (AFM) analysis showed p31-43 oligomers with different height distribution. Also, peptide concentration had a very strong influence on peptide self-organization process. Oligomers gradually increased their size at lower concentration. Whereas, at higher ones, oligomers increased their complexity, forming branched structures. By Circular Dichroism, we observed that p31-43 self-organized in a poly-proline II conformation in equilibrium with β-sheets-like structures, whose pH remained stable in the range of 3 to 8. In addition, these findings were supported by Molecular Dynamics Simulation. The formation of p31-43 nanostructures with increased β-sheet structure may help to explain the molecular etiopathogenesis in the induction of pro-inflammatory effects and subsequent damage at the intestinal mucosa in CeD.

Introduction

Gliadins and glutenins are proteins present in wheat, that form a viscoelastic structure, called gluten, through non-covalent interactions and disulphide bond exchange in the presence of water [1]. This protein complex has been extensively studied due to its technological properties in food manufacture, and because its consumption triggers Celiac Disease (CeD) in genetically predisposed individuals [2]. CeD is a highly prevalent chronic immune-mediated enteropathy which occurs in 1% of worldwide population, characterized by damage to small intestinal mucosa due to an exacerbated immune response by overactivation of gluten-specific T lymphocytes [3].

Gliadins are the ethanol-soluble fraction of gluten which can be separated by gel electrophoresis at acid pH in α/β-, γ-, and ω-gliadins [4]. The primary structure of gliadins has several repetitive sequences rich in proline and glutamine residues. These proteins are resistant to degradation by gastrointestinal enzymes, and consequently, several long peptides may remain in the gut lumen [5]. Different mechanisms have been suggested for their translocation into the mucosa of the small intestine, where they exhibit immunogenic properties through binding to HLA class II molecules becoming T cell epitopes [6, 7]. Among wheat proteins, peptides from α-gliadins are the most studied. The peptide 56-87 from α-gliadin fraction, called 33mer, has been extensively studied as model of T cell epitope because it induces an strong adaptive immune response in CeD patients [8], whereas the α-gliadin peptide p31-43, induces a non-HLA mediated inflammatory response as well as several toxic effects evaluated by *ex vivo* and *in vitro* assays [9-12]. Using an experimental model developed by our group, the *in vivo* biological effects of p31-43 have been recently studied [13, 14]. We observed that wild type mice treated with p31-43 presented histological alterations and increased number of intraepithelial lymphocytes, production of proinflammatory mediators and cell death. We also demonstrated that biological effects depend on the activation of the NLRP3 inflammasome [14]. In the other hand, Villella et.al [15] showed that p31-43 is capable of inhibiting the cystic fibrosis transmembrane conductance regulator (CFTR) and reduces ATPase activity of the nucleotide-binding domain-1 (NBD1) impairing its function. This generates epithelial stress, tissue transglutaminase and inflammasome activation, NF-κB nuclear translocation and IL-15 production. Considering that the activation of the inflammasome platform has been linked to the detection of nanostructures, fibrils and particulate material and damage

signals [16, 17], we hypothesize that p31-43 self-assembling properties may be critical to its biological effects.

Though, biological effects triggered by p31-43 (LGQQQPFPPQQPY) are observed very rapid upon treatment, the surface cell receptor or the mechanism of peptide entry have not been identified [18]. In our previous study, we showed by Circular Dichroism (CD) and Transmission Electron Microscopy (TEM) that p31-43 presents a poly-proline II (PPII) structure and forms oligomers which may promote the activation of the inflammasome platform [14]. To gain structural details on p31-43, several spectroscopic and microscopic techniques were used, as well as, coarse-grained dynamic simulation in order to understand at a molecular level, peptide interactions and driven forces that leads to p31-43 self-assembly.

Results

Characterization of p31-43 oligomers by Spectroscopic and Atomic Force Microscopy techniques.

In a previous report, we showed by TEM that p31-43 self-aggregates presenting a PPII structure, in agreement with CD determinations [14]. Subsequent NMR experiments performed by Calvanese L. *et al.* [19] confirmed that this peptide is able to adopt this structure.

To further evaluate the self-assembly propensity of p31-43 and the characteristics of the oligomers [14], we decided to use a variety of biophysical tools. Firstly, we used a fluorescent probe containing a boron dipyrromethane scaffold (BODIPY) [20]. The molecule used in this work is able to sense the presence of particular hydrophobic patches that can be generated by the presence of oligomeric structures. This probe was used to evaluate the self-aggregation of the β-amyloid peptide, detecting oligomers prior to the formation of fibrils which could not be detected by other probes [21]. When this probe binds to a specific site, an increment of its fluorescence intensity is detected at approximately 540 nm when sample is excited at 525 nm. Thus, to analyze if p31-43 can self-assemble in solution, we measured fluorescence emission spectra at different peptide concentrations (10, 50 and 100μM) in presence of 1μM BODIPY. A concentration-dependent increase in the fluorescent signal was observed, suggesting that, at higher

concentration, more binding sites were available. These results support the existence of p31-43 soluble oligomers in the range from 10 to 100µM **(Figure 1A).**

Furthermore, Dynamic Light Scattering (DLS) was used to detect structures in solution. In this study, we evaluated p31-43 at 125µM. This concentration was chosen because samples at lower concentrations lack of detectable dispersion. The solution presented high polydispersity, suggesting the presence of different oligomer populations in the sample. Two main populations were observed, one of 107±7.5nm of hydrodynamic diameter and big aggregates with an average diameter of 493±31nm **(Figure 1B)**. These findings prompted us to propose that, at this concentration, p31-43 oligomers are in equilibrium with larger nanostructures**.**

In our previous study, by using Circular Dichroism (CD) and Transmission Electron Microscopy (TEM), we demonstrated that p31-43 presents a PPII structure and forms oligomers which may promote the activation of the inflammasome platform [14]. Herein, we explored the self-assembly process of p31-43 by Atomic Force Microscopy as complementary technique, which allows a deeper evaluation of the morphology of the oligomers because of its higher resolution achieved in a hydrated environment. This tool provides a topographic image of the sample [22], providing a visualization of p31-43 self-assembly with minimum interference [23-25]. This methodology was previously used to understand the self-association process of different proteins and peptides such as β-amyloid [26] and 33-mer gliadin peptide [27] and protein such as α-synuclein [28], the silk protein [29], elastomeric ones as resilin [30] and it has been widely used to characterize protein complexes, oligomers and fibers [31]. In this case, 5, 50 and 100µM p31-43 solutions were prepared to cover the same range of concentrations used in previous *in vivo* assays (6,5 y 65µM). The samples were freshly prepared to avoid a time-dependence effect [32].

At 5µM final concentration, p31-43 self-assembled as isolated spherical oligomers randomly distributed on the mica surface with different heights (**Figure 2A**). When a height distribution and statistical analysis of the whole sample deposited in mica was performed, we found that most of the structures were of 2.6±2.08nm height average **(Figure 3A),** with a minor proportion of oligomers having higher values. The high standard deviation indicated the presence of different oligomers, as it was detected by cross section analysis of the aggregates (indicated with white arrows in **Figure 2A and 2B**). Oligomers presented different heights that were divided into three groups: 1.2; 2.25 and 3.25nm, suggesting that these species may be in equilibrium among each other. When the 50µM p31-43 solution

was analyzed, we observed diverse oligomer populations (**Figure 2C and 2D**), indicating that different species are in equilibrium. Most oligomeric structures presented a mean height of 5±3nm (**Figure 3B**). In this case, we observed three kinds of round shaped species with a height around 2.4, 4 and 10nm. Interestingly, higher structures of 20-60nm were detected. This suggests that some precipitation of soluble species may have been occurred. Finally, we analyzed a 100µM solution were clusters of small height, as well as, amorphous aggregates with approximately lengths of 250nm were observed (**Figure 2E**), having widths of 100-140nm and heights of 5nm (**Figure 2F**). Considering that the height of these aggregates was in the range of the oligomers observed in the 50µM sample, we propose that they were produced by lateral association of oligomers.

Gliadin p31-43 peptide presents a poly-proline II conformation in equilibrium with extended structures.

We aimed to evaluate whether the structure of p31-43 was affected by different physiological pHs that resemble the ones of the gastrointestinal tract. This is a relevant issue because despite the absence of ionizable side chains in the p31-43 sequence, the C-terminal carboxylates are generally expected to be protonated at pH values near 3.3. To this end, we assessed the secondary structure by CD in 20mM phosphate buffer at pHs: 3.0, 5.0, 7.4, 8.0 at 50µM final peptide concentration in MilliQ water (**Figure 4**). In our previous work, we demonstrated that p31-43 presents a PPII structure at 4ºC [14] which was also observed for other gliadin peptides such as the 33-mer gliadin peptide [33]. As this conformation is always in equilibrium with other structures and it has been shown that PPII is more populated at low temperatures [34-36] we selected 4°C as the one to study pH dependence on the peptide conformation. Herein, we confirm that p31-43 presents a PPII structure which remains stable at different pHs.

Aimed to get further details on the self-organization process of p31-43, we reanalyzed the conformations of the oligomers obtained performing coarse-grained (CG) simulations [14]. As shown in **Figure 5A**, p31-43 peptides undergo spontaneous oligomerization in aqueous solution, as evidenced by a decrease in the radius of gyration from 10nm i.e., half the maximum distance between peptides in the initial configuration of the simulation to 3.1nm that corresponds to the final radius of the 50-mer. Once a compact state is reached, the N- and C-terminal moieties remain close to each other forming intra and intermolecular salt bridges that optimize electrostatic interactions among different peptides (inset in **Figure 5A**). The formation of salt bridges contributes to decrease the pKa of the C-termini. Indeed, calculating the pKa of all carboxylates along the simulation

for the former oligomer shows a clear shift to lower pH than expected for a single carboxylate in solution (**Figure 5B**), explaining the absence of pH dependence observed in the CD experiments.

Next, we studied the peptide structure in a wider range of concentrations from 10 to 500μM. We observed a characteristic PPII structure signal [34] determined by a negative band near 203nm and a positive band at 225nm, at 4°C throughout all concentrations **(Figure 6A)**. Interestingly, when the p31-43 peptide concentration is increased, a hypochromic displacement of the negative band occurs, that is characteristic of a self-assembly process. In line with this, the secondary structure content calculated along dynamic simulations suggested that the aggregation process induced a small increase in PPII conformation in two central Prolines, as well as, in β-sheet conformation spread along the non-Proline amino acids (**Figure 6C and 6D).** A secondary structure analysis per aminoacid of the monomeric and oligomeric states, identified a structured segment located in the central portion of the peptide, which could account for the phenomenon observed in CD experiment. As the simulation progressed and the oligomer was formed, an increment of 28% of the PPII conformation was observed in residues Pro8 and Pro9, while more external aminoacids experienced an increase in the β extended conformation stabilized by the formation of β-sheets among other peptides in the oligomer.

To study the effect of temperature over p31-43 structure, we performed CD experiments at four different temperatures increasing from 4°C to 37°C (**Figure 6B**). We observed that the negative band had a hypochromic behavior with a displacement from 203nm to 205nm and the positive band at 225nm reduced its signal. These features along with the presence of an isodichroic point at 210nm, indicate that the PPII structure is in equilibrium with extended structures such as β-turns and β-sheet, due to the close proximity of the dihedral angles in the conformational landscape [34-35]. To confirm this behavior, we used the BestSel server [37] which analyses CD spectra and gives an overall idea of the percentage of each structure in the whole peptide population at different conditions. The analysis of the 4°C spectra by this server indicated that around 60% of the signal corresponded to structures as PPII, 18% are turns and 22% are anti-β strand. The same analysis for the 37°C spectra, showed that the PPII-like structures decreased to a 56% and the anti-β strand increase up to 26%. Moreover, as CD spectra could be considered the result of a combination of different structures, the mathematical *spectrum* subtraction of a protein at different conditions is an adequate tool to evaluate conformational transitions [38]. To confirm these findings, we subtracted the spectra

between 37°C and 4°C and observed a negative band at 220nm and a positive one at 200nm, indicating that at physiological temperature, the p31-43 peptide has an increase of the β-sheet like conformation (**Figure 6E**). At lower temperatures, the peptide had a PPII structure, whereas at 37 °C there was an increment of the β-sheet like one component. However, the PPII structure remained as the most representative.

The PPII conformation is stable in the presence of chaotropic agents such as urea and guanidinium chloride [39]. To evaluate whether these agents were able to modify the p31-43 structure, 50μM and 200μM p31-43 solutions were dissolved in presence of 8M urea. At both concentrations, a positive band was observed at 225nm that confirms the PPII structure of p31-43 (**Figure 6C**).

On the other hand, to confirm that the species were in conformational equilibrium, a 200μM p31-43 solution was incubated in the presence of trifluorethanol (TFE) (**Figure 6D**). This co-solvent is used to favor intramolecular bonds, such as the ones present in α-helix and β-sheets [40]. A hypochromic displacement of the negative band from -11000 to -6000 was observed when TFE concentration was increased from 0% to 50% together with a small red shift from 203nm to 205nm. Interestingly, the positive band at 225nm decreased when TFE was added, also an isodichroic point a 210nm was observed, suggesting that species may alternate between PPII conformation and extended structure. At TFE 50%, the positive band at 195nm and the red shift at 208nm suggested that p31-43 was in equilibrium with β-sheet like structures. Also, when the spectra of TFE 0% and 50% were analyzed using BestSel server, we detected a decrease of PPII-like structures from 60% to 50%, and an increase of the anti-parallel β-structure from 23% to 29%. This result was also confirmed by the mathematical subtraction of CD spectra between 50% and 0% TFE, which showed a characteristic β-sheet like structure (**Figure 6F**). Though, these findings suggest that p31-43 has mainly a PPII structure in equilibrium with β-sheet like structures, which depends on its self-assembly and the polarity of the environment.

Self-assembly process of p31-43 depends on peptide concentration.

Protein oligomerization and aggregation is a highly time and temperature dependent process, among other factors. Therefore, we run a series of assays to study p31-43 self-assembling in a period of 7 days. For that, p31-43 solutions were incubated at 4 ºC, to diminish the ongoing aggregation reaction and preserve the first stages of the peptide self-assembly as it was done for polyglutamine proteins [41]. In this study, we evaluated the

morphological change of p31-43 oligomerization by AFM. A similar methodology was previously performed to evaluate the self-assembly process of proteins as the serum amyloid A1.1 [42], fibrils from the bacterial protein MinE [43] and the hen egg lysozyme [44]. We evaluated two peptide concentrations, 10μM and 50μM. At concentrations higher than 100μM, a full coverage of the surface was observed; therefore, it was not possible to evaluate the system by AFM.

Analysis of a freshly prepared 10μM sample deposited on mica surface showed three populations of oligomers. The smaller ones had an average height of 2.61±0.54 nm, composed by 3-4 monomers, the intermediate ones of 4.71±0.86 nm height with 5-6 monomers per oligomer and higher ones of 6.259±0.71nm height composed by 8-10 monomers. The higher and the smaller ones were in minor proportion as shown in **Figures 7A** and **8A**. It is worth to mention that the oligomers detected at 10μM were bigger than the ones observed at 5μM, thus confirming that the self-organization process depends on peptide concentration.

Next, the sample was incubated for 4 days at 4°C and deposited on the mica surface. At this condition, peptide oligomers self-associated generating larger isolated clusters with an average height of 5.56±0.96nm. These values indicate that the initial oligomers observed in **Figure 7A,** associated to form plane-cluster like structures (**Figure 7B** and **Figure 8B)**. These wider planar cluster (with approximately 32 monomers) may be generated by self-association of the smaller ones presented in **Figure 8C**. This finding allowed us hypothesizes a colloidal behavior of p31-43 peptide.

Spherical oligomers were detected after a continuous incubation of 7 days. However, there were no planar-cluster assemblies (**Figure 7C**). These spherical oligomers are higher than the planar clusters and had an average height of 22.2±8.2nm. This indicates that the oligomers observed in **Figure 7B** might be produced by rearrangement of wider structures, producing higher stable spherical structures which have less surface exposure, as it was previously observed in other systems [45, 46].

When the self-organization process was analyzed in 50μM peptide solutions, the structures observed differed from the ones detected at 10μM, confirming that this process is dependent on peptide concentration. In the freshly prepared sample, small and higher spherical oligomers were detected (**Figure 9A and 10A**). The smaller oligomeric structures average height was 4.1±1.6nm (approximately 6-8 monomers per oligomer) whereas the bigger ones were 18±6.3nm (10-14 monomers per oligomer). Also, some

structures had heights of 50nm, similar to Figure 2. These could have been produced by some precipitation that might occur during the deposition. This was observed in all three samples prepared at different times.

After a 4 day-incubation of the sample at 4°C the spherical oligomers arranged as a chain-like fractal network. Interestingly, in this structure, little individual oligomers were detected, since most of the peptide is forming these new linear structures. The smaller oligomers had an average of 8.07±4.13nm and the bigger ones were approximately 21.47±5.47nm height (12-20 monomers per oligomer). For this structure, the fractal dimension (D_f) which described the self-similarity of the system was calculated. Using the box counting method as it is described in the **SI,** we obtained a D_f of 1.4 (**Figure 9B)**. This characteristic self-organization ability of p31-43 was also observed for the silicatenin protein [47] and the 33-mer gliadin peptide [27, 48].

After incubating the sample at 4°C for 7 days, the linear chain network described above, continued evolving forming longer linear structures like fractals with an average height of 14.53±6.71nm. Interestingly, no individual oligomers were distinguished in this structure, suggesting that they may have interacted with each other to form the small linear structures detected. However, some large clusters with a height of 40.33±6.5nm could be observed, which might have been generated by some precipitation (**Figure 9C**). When D_f was calculated, a value of 1.7 was obtained, suggesting that, at this time, the structures were formed by a diffusion limited aggregation (DLA) mechanism. By this theory, the peptide is described as a colloidal particle in which every particle collision leads to an irreversible association and formation of a fractal structure, which has a typical D_f value of 1.7-1.8 [29, 47, 49].

Discussion

Celiac disease (CeD) is a common gastrointestinal disease triggered by dietary gluten peptides. Though, the specific immune response against a group of immunogenic peptides is well established, the role of gliadin peptides in the induction of inflammatory responses is less understood [12, 13]. The p31-43 gliadin peptide, generated by digestion of gastrointestinal and brush border enzymes, is the most used model peptide to evaluate the innate immune response in CeD [9]. Using an experimental model in mice, we have shown that p31-43 induces local inflammatory responses and increased cell death in small intestine, which requires MyD88 and type I IFN pathways [13]. Further *in vivo* assays showed that the innate response depends on the NLRP3 inflammasome [14], and its

capacity to sense signals derived from cell damage produced by nanostructures or by direct interaction with these species [16, 17, 50]. By CD and TEM, we showed that p31-43 is able to form oligomers in the multinanometer scale [14]. Since a cell surface receptor for p31-43 has not been identified [18], we hypothesize that structural features of p31-43 may be of key importance in the induction of different biological effects.

Fluorescence spectroscopy and DLS allowed assessing whether the self-organization process occurs in solution. A fluorescent probe called BODIPY, which was previously employed to detect oligomers of β42 amyloid peptide was used [21]. The fluorescence signal of this probe in presence of p31-43 suggests that oligomers with hydrophobic patches are presented in solution. The oligomer size increased at higher peptide concentrations as it was detected in the spectra. In addition, DLS measurements confirmed that higher ordered and stable structures were present in solution (**Figure 1**). This result is in concordance with our CD studies performed at a wide range of concentrations which showed a self-assembly behavior (**Figure 6A**). This process was also previously described in elastomeric proteins such as lamprim [51], elastin II fragments [38, 52] and the 33-mer gliadin peptide [27,33,48].

The AFM analysis confirmed that p31-43 oligomerizes and the size of the oligomers and the structures observed are dependent on peptide concentration. Results obtained at 5μM and 50μM, showed spherical nanostructures with different heights that were in equilibrium with each other. However, at 50μM some bigger oligomers and precipitation was detected. We hypothesize that, at these concentrations, p31-43 behaves as a colloid nanostructure where each spherical oligomer tends to interact with each other as it was observed in terminal fragments of serum amyloid A [42]. At 100μM, the peptide generates clusters and amorphous aggregates in solution that may be deposited on the mica. These structures have an average height similar to the oligomers at 50μM (**Figure 2**), suggesting that p31-43 self-assembles to generate these structures. This behavior was also observed for the β-amyloid peptide [53] which is typical for colloidal structures at high concentration [49]. It is worth to mention that these structures are in concordance with our previous observations by TEM confirming that p31-43 self-assembles into oligomers and clusters.

CD analysis showed that p31-43 presented PPII secondary structure, which was also recently confirmed by NMR experiments [19]. Since this conformation lacks of intrachain hydrogen bonds and is fully hydrated in aqueous solution [54], PPII helix has the

appropriate characteristics to be in equilibrium with other conformations. In fact, evaluation of the peptide at 200μM solution at different temperatures, showed a conformational transition from PPII to β-sheet like structures as it was inferred by both the use of BestSel and difference spectra, and supported by molecular simulations. The treatment of 200μM and 50μM solutions with urea returns p31-43 to a PPII conformation while TFE, a co-solvent that favors hydrogen bonds, produced 50% of a β-sheet like signal (**Figures 6B, C and D**). These observations strongly suggest that the peptide is in equilibrium with extended and folded structures at physiological temperatures. Similar behavior was observed in other proteins and peptides such as the amyloidogenic exon-30 of tropoelastin [35]. The same self-association propensity was confirmed at the molecular level by the coarse-grained molecular dynamics simulations of a monomer in a box containing 50 replicas.

When the p31-43 was studied at different pHs by CD and MD, no structural transitions were observed, indicating that its structure it is not affected by changes in pH in the range of 3 to 8. Analysis of the oligomeric state obtained by simulations indicated that the formation of salt bridges between terminal zwitterionic moieties is determinant for pH stability, shifting C-terminal values to acidic conditions in almost one pKa unit. These findings suggest that the aggregation process might contribute to the resistance of properties of p31-43 would not be affected by changes in pH along the gastrointestinal tract and in the small intestinal mucosa.

To get further insight into the self-assembly behavior of p31-43, we performed an AFM evaluation, assessment already used to understand protein aggregation, as it was done for the polyalanine expansion of PHOX2B aggregation [55]. We observed that p31-43 self-assembly process showed different behavior depending on the peptide concentration as described for the β-amyloid peptide [56] and the N-terminal serum amyloid A peptides [57]. We hypothesize that the peptide behaves as a colloidal nanoparticle that could self-associate depending on its concentration. At the lower concentration, the small colloidal particles, following a self-association process, produce planar clusters that then reorganize into spherical bigger oligomers. Since small oligomers co-exist with bigger ones and bigger structures are detected over time, we propose that this process is driven by an Ostwald ripening like process [58, 59].

At 50μM p31-43 self-organize differently, the peptide structure changes from spherical oligomers to a chain network accompanied by some individual ones. After 7

days, this behavior progresses to large branched structures with a fractal morphology and a D_f *~1.7* suggesting a DLA mechanism. This self-organization behavior was previously detected in 33-mer gliadin peptide [27,33,48] and whey proteins [60, 61]. Peptide concentration could strongly influence the type of interactions established among monomers leading to differences in the self-assembly behavior [49]. Based on these findings, a scheme of self-assembly process is proposed (**Figure 11**).

The driven forces of the self-organization of p31-43 may be explained by its high content of glutamines. In poly-glutamine sequences, the formation of oligomers and higher ordered structures is a consequence of the hydrophobic effect and specific hydrogen bonds generated among monomers [62]. In the case of p31-43, an uncharged peptide, both intermolecular forces might be the key drivers of the self-assembly characteristic [63]. However, the formation of oligomers does not preclude that p31-43 may act also as monomer. Recent work by Villela *et al*. [15] showed that monomeric p31-43 binds to the NBD1 subunit of the chloride channel (cystic fibrosis transmembrane conductance regulator, CFTR) and inhibit its function. As consequence, autophagy is altered, and NFκB and inflammasome pathways are activated, producing the release of inflammatory mediators.

Conclusion

In conclusion, considering that the surface cell receptor or the mechanism of peptide entry have not been identified, and recently *in silico* analysis suggested that p31-43 does not bind to HLA class II molecules [19], our findings open a new perspective to understand the biological effects of this peptide in the induction of inflammatory and cell death pathways. As a monomer, it can mediate selective effects as, the recently shown, inhibition of the subunit of the chloride channel. Oligomers, in turn, may play a role in the multiple and fast non-HLA mediated mechanisms, like altering vesicular trafficking and cellular stress [12], and our own work on the activation of NLRP3 inflammasome [14]. Altogether, these findings help to understand the innate immune response elicited as supplementary events in triggering celiac disease.

Materials and Methods

1. Sample preparation

The p31-43 peptide was purchased from GeneCust (Luxembourg). The peptide was dissolved in Milli Q water generating a mother solution of 600 µM which was stored at -20 ºC. From this mother solution the working samples were prepared before the measurements and stored on ice. Meanwhile experiments were carried out, the samples were kept on ice to avoid effects of temperature on the peptide conformation.

The kinetic assay was performed by preparing peptide dilutions from the stock solution to the desired concentration (10 and 50 µM) and incubating them at 4 ºC for 0 (fresh solution), 4, 7 and 14 days in a cold room, on ice, before deposition on the mica surface.

For reproducibility, three different peptide batches were used for the experiments presented in this work. The concentration dependent experiments solutions at 10, 50, 200 and 500µM in MilliQ water were prepared.

For the CD experiments in Urea 8M the peptide mother solution was directly dissolved in an adequate urea concentration solution to achieve the final urea concentration required. The sample was incubated 3 hours to reach the equilibrium. The Trifluorethanol titration experiment (TFE) was performed on cuvette and the concentration of the peptide was recalculated in each titration step the sample was incubated 10 minutes before data acquisition. The kinetic assay was performed by preparing peptide solutions from the mother one to the desired concentration and incubating it at 4ºC at 0 (fresh solution), 4, 7 and 14 days in a cold room and ice before the deposition on the mica surface.

2. Fluorescence Spectroscopy

The emission spectra of p31-43 in presence of BODIPY probe was performed in a JASCO FP 8300. In this case, Milli Q water solution of the peptide at the concentration 10, 50 and 100µM were freshly prepared and BODIPY probe was added at 1µM final concentration. Also, we used water as control. Then, the emission spectrum of each sample was obtained by exciting the samples at 525nm wavelength and the slits used were 5nm for the excitation and emission.

3. Dynamic Light Scattering

Samples of p31-43 gliadin peptide were dissolved on water and filtered with a 200nm filter to eliminate big oligomers/ aggregates and dust. Then the measures were performed by

triplicate using a Zetasizer (Nano-ZS) from Malvern Instruments and the analysis of the autocorrelation functions obtained was performed by Dispersion Technology Software (DTS) from Malvern.

4. Atomic Force Microscopy

All images to characterize the peptide self-assembly were obtained in Tapping mode AFM with MultiMode Scanning Probe Microscope (Nanoscope V; Bruker, Santa Barbara, CA) equipped with a Nanoscope V controller (Veeco, Santa Barbara, CA, USA), using probes doped with silicon nitride (RTESP, Veeco with tip nominal radius of 8 -12 nm, 271e311 kHz, force constant 20-80 N m-1). Typical rate scanners were 1 Hz.

Water aqueous solutions of the peptides at concentrations from 10, 50 and 100μM were deposited on freshly cleaved mica, and left to interact with the surface for five minutes at room temperature. Then the samples were dried by a Nitrogen flow. The height of the observed architectures was determined by cross section using Nanoscope Analysis 1.40 software (Bruker).

5. Circular Dichroism

CD spectra of peptide solutions at were recorded on a Jasco J-810 CD spectropolarimeter using a Peltier system as temperature controller. For this experiment five scans were acquired in the range of 190–250nm at a selected temperature (from 4ºC to 37ºC with an incubation of 10 minutes for each measurement). The scanning speed of 50nm per minute was used. The spectra were obtained employing a 1-mm and 0.1-mm quartz cuvettes. Blank scans were subtracted from the spectra. The data were expressed as the mean residue molar ellipticity in deg cm^2 $dmol^{-1}$. Smooth noise reduction was applied eventually when it was necessary using a binomial method. Graphics were represented using the program Origin (OriginLab).

6. Molecular simulations

Molecular dynamics simulations were performed at the coarse grained level using the SIRAH force field [14, 64] at 37 ºC and 1 atm with no added salt to mimic the conditions of circular dichroism experiments (see above). Oligomerization was simulated by introducing 50 replicas of the isolated, zwitterionic, peptide in different conformations randomly selected along a MD trajectory of an isolated peptide. The simulation of the oligomer was performed for 5μs. To ensure no aggregation bias in the initial spatial distribution, isolated

peptides were placed in random conformations within a computational box leaving at least 4nm between each replica. Secondary structure and atomistic structures from coarse-grained conformers were calculated using SirahTools [65]. Secondary structure contents per aminoacid were averaged over the last 100ns of the trajectory. pKa values on C-terminal moieties were calculated with PropKa [66] using the pdb2pqr server [67] on 10 conformers taken from the last 100ns of simulation.

7. Fractal Dimension:

Fractal Dimension is a measure of the complexity of a system. It is a scaling rule that is used to compare how pattern details change when the scale varied from minor to major resolution. Mathematically, it is expressed as

$$N \propto \epsilon^{-Df}$$

Where D_f is the fractal dimension, N is the number of pieces observed in each new resolution and ϵ is the scale used for each pieces.

FracLac software from Image J was employed for the determination of D_f using the box counting procedure. The basic procedure is to lay systematically a series of grids of decreasing calibre (the boxes) over an image and record data (the counting) for each successive calibre. The program gives access to D_f obtained by the application of several mathematical algorithms.

Author Contributions:

MFGC and MGH performed spectroscopic experiments. EP performed AFM. SP and EB performed molecular dynamic simulation. FC, MGH and MFGC designed the experiments. VI, MGH and MFGC analyzed the data. MFGC, MGH, SP, VI and FC wrote the manuscript

Acknowledgement:

We would like to thank Dr. Nicolo Tonelli (Laboratoire de Toxinologie Moléculaire et Biotechnologies (LTMB), Gif-sur-Yvette, France) who kindly provide the fluorescent probe BODIPY, which he synthesized.

This work was supported by CONICET (National Scientific and Technical Research Council), ANCyPT (National Agency for Promotion of Science and Technology) (PICT2015 1246), UNLP (Universidad Nacional de La Plata). MFGC is the beneficiary of a doctoral

fellowship of CONICET (Consejo Nacional de Investigaciones Científicas y Técnicas, Argentina). MGH and EB are the beneficiary of a postdoctoral fellowship of CONICET (Consejo Nacional de Investigaciones Científicas y Técnicas, Argentina)

Conflict of interest

The authors declare no conflict of interest.

References

1. Wieser, H. (2007) Chemistry of gluten proteins, *Food microbiology.* **24**, 115-9.
2. Lebwohl, B., Sanders, D. S. & Green, P. H. R. (2018) Coeliac disease, *The Lancet.* **391**, 70-81.
3. Hardy, M. Y. & Tye-Din, J. A. (2016) Coeliac disease: a unique model for investigating broken tolerance in autoimmunity, *Clinical & translational immunology.* **5**, e112.
4. Rumbo, M., Chirdo, F. G., Giorgieri, S. A., Fossati, C. A. & Añón, M. C. (1999) Preparative Fractionation of Gliadins by Electrophoresis at pH 3.1 (A-PAGE), *Journal of Agricultural and Food Chemistry.* **47**, 3243-3247.
5. Shan, L., Qiao, S.-W., Arentz-Hansen, H., Molberg, Ø., Gray, G. M., Sollid, L. M. & Khosla, C. (2005) Identification and Analysis of Multivalent Proteolytically Resistant Peptides from Gluten: Implications for Celiac Sprue, *Journal of Proteome Research.* **4**, 1732-1741.
6. Petersen, J., Montserrat, V., Mujico, J. R., Loh, K. L., Beringer, D. X., van Lummel, M., Thompson, A., Mearin, M. L., Schweizer, J., Kooy-Winkelaar, Y., van Bergen, J., Drijfhout, J. W., Kan, W. T., La Gruta, N. L., Anderson, R. P., Reid, H. H., Koning, F. & Rossjohn, J. (2014) T-cell receptor recognition of HLA-DQ2-gliadin complexes associated with celiac disease, *Nature structural & molecular biology.* **21**, 480-8.
7. Kooy-Winkelaar, Y., van Lummel, M., Moustakas, A. K., Schweizer, J., Mearin, M. L., Mulder, C. J., Roep, B. O., Drijfhout, J. W., Papadopoulos, G. K., van Bergen, J. & Koning, F. (2011) Gluten-specific T cells cross-react between HLA-DQ8 and the HLA-DQ2alpha/DQ8beta transdimer, *Journal of immunology.* **187**, 5123-9.
8. Qiao, S.-W., Bergseng, E., Molberg, Ø., Xia, J., Fleckenstein, B., Khosla, C. & Sollid, L. M. (2004) Antigen Presentation to Celiac Lesion-Derived T Cells of a 33-Mer Gliadin Peptide Naturally Formed by Gastrointestinal Digestion, *The Journal of Immunology.* **173**, 1757-1762.
9. Gianfrani, C., Auricchio, S. & Troncone, R. (2005) Adaptive and innate immune responses in celiac disease, *Immunology letters.* **99**, 141-5.
10. Barone, M. V., Troncone, R. & Auricchio, S. (2014) Gliadin peptides as triggers of the proliferative and stress/innate immune response of the celiac small intestinal mucosa, *International journal of molecular sciences.* **15**, 20518-37.
11. Maiuri, L., Troncone, R., Mayer, M., Coletta, S., Picarelli, A., De Vincenzi, M., Pavone, V. & Auricchio, S. (1996) In vitro activities of A-gliadin-related synthetic peptides: damaging effect on the atrophic coeliac mucosa and activation of mucosal immune response in the treated coeliac mucosa, *Scandinavian journal of gastroenterology.* **31**, 247-53.
12. Nanayakkara, M., Lania, G., Maglio, M., Auricchio, R., De Musis, C., Discepolo, V., Miele, E., Jabri, B., Troncone, R., Auricchio, S. & Barone, M. V. (2018) P31–43, an

undigested gliadin peptide, mimics and enhances the innate immune response to viruses and interferes with endocytic trafficking: a role in celiac disease, *Scientific Reports.* **8**, 10821.
13. Araya, R. E., Gomez Castro, M. F., Carasi, P., McCarville, J. L., Jury, J., Mowat, A. M., Verdu, E. F. & Chirdo, F. G. (2016) Mechanisms of innate immune activation by gluten peptide p31-43 in mice, *Am J Physiol Gastrointest Liver Physiol.* **311**, G40-9.
14. Gómez Castro, M. F., Miculán, E., Herrera, M. G., Ruera, C., Perez, F., Prieto, E. D., Barrera, E., Pantano, S., Carasi, P. & Chirdo, F. G. (2019) p31-43 Gliadin Peptide Forms Oligomers and Induces NLRP3 Inflammasome/Caspase 1- Dependent Mucosal Damage in Small Intestine, *Frontiers in Immunology.* **10**.
15. Villella, V. R., Venerando, A., Cozza, G., Esposito, S., Ferrari, E., Monzani, R., Spinella, M. C., Oikonomou, V., Renga, G., Tosco, A., Rossin, F., Guido, S., Silano, M., Garaci, E., Chao, Y. K., Grimm, C., Luciani, A., Romani, L., Piacentini, M., Raia, V., Kroemer, G. & Maiuri, L. (2019) A pathogenic role for cystic fibrosis transmembrane conductance regulator in celiac disease, *The EMBO journal.* **38**.
16. Nakanishi, A., Kaneko, N., Takeda, H., Sawasaki, T., Morikawa, S., Zhou, W., Kurata, M., Yamamoto, T., Akbar, S. M. F., Zako, T. & Masumoto, J. (2018) Amyloid beta directly interacts with NLRP3 to initiate inflammasome activation: identification of an intrinsic NLRP3 ligand in a cell-free system, *Inflammation and regeneration.* **38**, 27.
17. Gomez, D. M., Urcuqui-Inchima, S. & Hernandez, J. C. (2017) Silica nanoparticles induce NLRP3 inflammasome activation in human primary immune cells, *Innate immunity.* **23**, 697-708.
18. Paolella, G., Lepretti, M., Martucciello, S., Nanayakkara, M., Auricchio, S., Esposito, C., Barone, M. V. & Caputo, I. (2018) The toxic alpha-gliadin peptide 31–43 enters cells without a surface membrane receptor, *Cell Biology International.* **42**, 112-120.
19. Calvanese, L., Nanayakkara, M., Aitoro, R., Sanseverino, M., Tornesello, A. L., Falcigno, L., D'Auria, G. & Barone, M. V. (2019) Structural insights on P31-43, a gliadin peptide able to promote an innate but not an adaptive response in celiac disease, *Journal of peptide science : an official publication of the European Peptide Society.* **25**, e3161.
20. Ono, M., Watanabe, H., Kimura, H. & Saji, H. (2012) BODIPY-based molecular probe for imaging of cerebral beta-amyloid plaques, *ACS chemical neuroscience.* **3**, 319-24.
21. Smith, N. W., Alonso, A., Brown, C. M. & Dzyuba, S. V. (2010) Triazole-containing BODIPY dyes as novel fluorescent probes for soluble oligomers of amyloid Abeta1-42 peptide, *Biochemical and biophysical research communications.* **391**, 1455-8.
22. Last, J. A., Russell, P., Nealey, P. F. & Murphy, C. J. (2010) The applications of atomic force microscopy to vision science, *Investigative ophthalmology & visual science.* **51**, 6083-94.
23. Baclayon, M., Roos, W. H. & Wuite, G. J. (2010) Sampling protein form and function with the atomic force microscope, *Molecular & cellular proteomics : MCP.* **9**, 1678-88.
24. Dufrene, Y. F., Ando, T., Garcia, R., Alsteens, D., Martinez-Martin, D., Engel, A., Gerber, C. & Muller, D. J. (2017) Imaging modes of atomic force microscopy for application in molecular and cell biology, *Nature nanotechnology.* **12**, 295-307.
25. Lu, Z., Zhang, Z. & Pang, D. (2005) Atomic force microscopy in cell biology, *Chinese Science Bulletin.* **50**, 1409.
26. Antzutkin, O. (2017) Polymorphism of Alzheimer´s A-beta Amyloid Fibrils in *Modern Magnetic Resonance* (Graham, A. W. & Graham, A. W., eds) pp. 1-15, Springer International Publishing.
27. Herrera, M. G., Benedini, L. A., Lonez, C., Schilardi, P. L., Hellweg, T., Ruysschaert, J. M. & Dodero, V. I. (2015) Self-assembly of 33-mer gliadin peptide oligomers, *Soft matter.* **11**, 8648-60.

28. Fauerbach, J. A., Yushchenko, D. A., Shahmoradian, S. H., Chiu, W., Jovin, T. M. & Jares-Erijman, E. A. (2012) Supramolecular non-amyloid intermediates in the early stages of alpha-synuclein aggregation, *Biophysical journal.* **102**, 1127-36.
29. Greving, I., Cai, M., Vollrath, F. & Schniepp, H. C. (2012) Shear-induced self-assembly of native silk proteins into fibrils studied by atomic force microscopy, *Biomacromolecules.* **13**, 676-82.
30. Qin, G., Hu, X., Cebe, P. & Kaplan, D. L. (2012) Mechanism of resilin elasticity, *Nature communications.* **3**, 1003.
31. Bernini, F., Malferrari, D., Pignataro, M., Bortolotti, C. A., Di Rocco, G., Lancellotti, L., Brigatti, M. F., Kayed, R., Borsari, M., Del Monte, F. & Castellini, E. (2016) Pre-amyloid oligomers budding:a metastatic mechanism of proteotoxicity, *Sci Rep.* **6**, 35865.
32. Zagorski, M. G., Yang, J., Shao, H., Ma, K., Zeng, H. & Hong, A. (1999) [13] Methodological and chemical factors affecting amyloid β peptide amyloidogenicity in *Methods in Enzymology* pp. 189-204, Academic Press.
33. Herrera, M. G., Zamarreno, F., Costabel, M., Ritacco, H., Hutten, A., Sewald, N. & Dodero, V. I. (2014) Circular dichroism and electron microscopy studies in vitro of 33-mer gliadin peptide revealed secondary structure transition and supramolecular organization, *Biopolymers.* **101**, 96-106.
34. Bochicchio, B. & Tamburro, A. M. (2002) Polyproline II structure in proteins: identification by chiroptical spectroscopies, stability, and functions, *Chirality.* **14**, 782-92.
35. Tamburro, A. M., Pepe, A., Bochicchio, B., Quaglino, D. & Ronchetti, I. P. (2005) Supramolecular amyloid-like assembly of the polypeptide sequence coded by exon 30 of human tropoelastin, *The Journal of biological chemistry.* **280**, 2682-90.
36. Bochicchio, B., Pepe, A. & Tamburro, A. M. (2001) On (GGLGY) synthetic repeating sequences of lamprin and analogous sequences, *Matrix biology : journal of the International Society for Matrix Biology.* **20**, 243-50.
37. Micsonai, A., Wien, F., Bulyaki, E., Kun, J., Moussong, E., Lee, Y. H., Goto, Y., Refregiers, M. & Kardos, J. (2018) BeStSel: a web server for accurate protein secondary structure prediction and fold recognition from the circular dichroism spectra, *Nucleic Acids Res.* **46**, W315-W322.
38. Pepe, A. & Bochicchio, B. (2013) An Elastin-Derived Self-Assembling Polypeptide, *Journal of Soft Matter.* **2013**, 7.
39. Lopes, J. L., Miles, A. J., Whitmore, L. & Wallace, B. A. (2014) Distinct circular dichroism spectroscopic signatures of polyproline II and unordered secondary structures: applications in secondary structure analyses, *Protein science : a publication of the Protein Society.* **23**, 1765-72.
40. Sonnichsen, F. D., Van Eyk, J. E., Hodges, R. S. & Sykes, B. D. (1992) Effect of trifluoroethanol on protein secondary structure: an NMR and CD study using a synthetic actin peptide, *Biochemistry.* **31**, 8790-8.
41. Jayaraman, M., Thakur, A. K., Kar, K., Kodali, R. & Wetzel, R. (2011) Assays for studying nucleated aggregation of polyglutamine proteins, *Methods.* **53**, 246-54.
42. Srinivasan, S., Patke, S., Wang, Y., Ye, Z., Litt, J., Srivastava, S. K., Lopez, M. M., Kurouski, D., Lednev, I. K., Kane, R. S. & Colon, W. (2013) Pathogenic serum amyloid A 1.1 shows a long oligomer-rich fibrillation lag phase contrary to the highly amyloidogenic non-pathogenic SAA2.2, *The Journal of biological chemistry.* **288**, 2744-55.
43. Chiang, Y. L., Chang, Y. C., Chiang, I. C., Mak, H. M., Hwang, I. S. & Shih, Y. L. (2015) Atomic Force Microscopy Characterization of Protein Fibrils Formed by the Amyloidogenic Region of the Bacterial Protein MinE on Mica and a Supported Lipid Bilayer, *PloS one.* **10**, e0142506.

44. Crespo, R., Villar-Alvarez, E., Taboada, P., Rocha, F. A., Damas, A. M. & Martins, P. M. (2016) What Can the Kinetics of Amyloid Fibril Formation Tell about Off-pathway Aggregation?, *The Journal of biological chemistry.* **291**, 2018-32.
45. Levin, A., Mason, T. O., Adler-Abramovich, L., Buell, A. K., Meisl, G., Galvagnion, C., Bram, Y., Stratford, S. A., Dobson, C. M., Knowles, T. P. J. & Gazit, E. (2014) Ostwald's rule of stages governs structural transitions and morphology of dipeptide supramolecular polymers, *Nature communications.* **5**, 5219.
46. Ray, S., Singh, N., Pandey, S., Kumar, R., Gadhe, L., Datta, D., Patel, K., Mahato, J., Navalkar, A., Panigrahi, R., Chatterjee, D., Maiti, S., Bhatia, S., Mehra, S., Singh, A., Gerez, J., Chowdhury, A., Kumar, A., Padinhateeri, R., Riek, R., Krishnamoorthy, G. & Maji, S. K. (2019) Liquid-liquid phase separation and liquid-to-solid transition mediate α-synuclein amyloid fibril containing hydrogel formation, *bioRxiv*, 619858.
47. Murr, M. M. & Morse, D. E. (2005) Fractal intermediates in the self-assembly of silicatein filaments, *Proceedings of the National Academy of Sciences of the United States of America.* **102**, 11657-62.
48. Herrera, M. G., Pizzuto, M., Lonez, C., Rott, K., Hutten, A., Sewald, N., Ruysschaert, J. M. & Dodero, V. I. (2018) Large supramolecular structures of 33-mer gliadin peptide activate toll-like receptors in macrophages, *Nanomedicine : nanotechnology, biology, and medicine.* **14**, 1417-1427.
49. Crick, S. L. & Pappu, R. V. (2012). Thermodynamic and Kinetic Models for Aggregation of Intrinsically Disordered Proteins. In Pr*otein and Peptide Folding, Misfolding, and Non-Folding* (V. N. Uversky and R. Schweitzer Stenner eds), pp. 413-440. John Wiley & Sons.
50. Christo, S., Bachhuka, A., Diener, K. R., Vasilev, K. & Hayball, J. D. (2016) The contribution of inflammasome components on macrophage response to surface nanotopography and chemistry, *Scientific Reports.* **6**, 26207.
51. Robson, P., Wright, G. M., Sitarz, E., Maiti, A., Rawat, M., Youson, J. H. & Keeley, F. W. (1993) Characterization of lamprin, an unusual matrix protein from lamprey cartilage. Implications for evolution, structure, and assembly of elastin and other fibrillar proteins, *The Journal of biological chemistry.* **268**, 1440-7.
52. Tamburro, A. M., Guantieri, V., Pandolfo, L. & Scopa, A. (1990) Synthetic fragments and analogues of elastin. II. Conformational studies, *Biopolymers.* **29**, 855-70.
53. Jiang, D., Rauda, I., Han, S., Chen, S. & Zhou, F. (2012) Aggregation pathways of the amyloid beta(1-42) peptide depend on its colloidal stability and ordered beta-sheet stacking, *Langmuir : the ACS journal of surfaces and colloids.* **28**, 12711-21.
54. Blanch, E. W., Morozova-Roche, L. A., Cochran, D. A. E., Doig, A. J., Hecht, L. & Barron, L. D. (2000) Is polyproline II helix the killer conformation? a raman optical activity study of the amyloidogenic prefibrillar intermediate of human lysozyme11Edited by A. R. Fersht, *Journal of Molecular Biology.* **301**, 553-563.
55. Pirone, L., Caldinelli, L., Di Lascio, S., Di Girolamo, R., Di Gaetano, S., Fornasari, D., Pollegioni, L., Benfante, R. & Pedone, E. (2019) Molecular insights into the role of the polyalanine region in mediating PHOX2B aggregation, *The FEBS journal*.
56. Stine, W. B., Jr., Dahlgren, K. N., Krafft, G. A. & LaDu, M. J. (2003) In vitro characterization of conditions for amyloid-beta peptide oligomerization and fibrillogenesis, *The Journal of biological chemistry.* **278**, 11612-22.
57. Ahmed, I. & Jones, E. M. (2019) Importance of micelle-like multimers in the atypical aggregation kinetics of N-terminal serum amyloid A peptides, *FEBS letters.* **593**, 518-526.
58. Buell, A. K. (2017) The Nucleation of Protein Aggregates - From Crystals to Amyloid Fibrils, *International review of cell and molecular biology.* **329**, 187-226.

59. Armiento, A., Moireau, P., Martin, D., Lepejova, N., Doumic, M. & Rezaei, H. (2017) The mechanism of monomer transfer between two structurally distinct PrP oligomers, *PloS one.* **12**, e0180538.
60. Mahmoudi, N., Axelos, M. A. V. & Riaublanc, A. (2011) Interfacial properties of fractal and spherical whey protein aggregates, *Soft matter.* **7**, 7643-7654.
61. Inthavong, W., Kharlamova, A., Chassenieux, C. & Nicolai, T. (2016) Structure and flow of dense suspensions of protein fractal aggregates in comparison with microgels, *Soft matter.* **12**, 2785-2793.
62. Khare, S. D., Ding, F., Gwanmesia, K. N. & Dokholyan, N. V. (2005) Molecular origin of polyglutamine aggregation in neurodegenerative diseases, *PLoS computational biology.* **1**, 230-5.
63. Perutz, M. F., Johnson, T., Suzuki, M. & Finch, J. T. (1994) Glutamine repeats as polar zippers: their possible role in inherited neurodegenerative diseases, *Proceedings of the National Academy of Sciences.* **91**, 5355-5358.
64. Darré, L., Machado, M. R., Brandner, A. F., González, H. C., Ferreira, S. & Pantano, S. (2015) SIRAH: A Structurally Unbiased Coarse-Grained Force Field for Proteins with Aqueous Solvation and Long-Range Electrostatics, *Journal of Chemical Theory and Computation.* **11**, 723-739.
65. Machado, M. R. & Pantano, S. (2016) SIRAH tools: mapping, backmapping and visualization of coarse-grained models, *Bioinformatics.* **32**, 1568-1570.
66. Rostkowski, M., Olsson, M. H. M., Søndergaard, C. R. & Jensen, J. H. (2011) Graphical analysis of pH-dependent properties of proteins predicted using PROPKA, *BMC structural biology.* **11**, 6-6.
67. McCammon, J. A., Nielsen, J. E., Baker, N. A. & Dolinsky, T. J. (2004) PDB2PQR: an automated pipeline for the setup of Poisson–Boltzmann electrostatics calculations, *Nucleic Acids Research.* **32**, W665-W667.

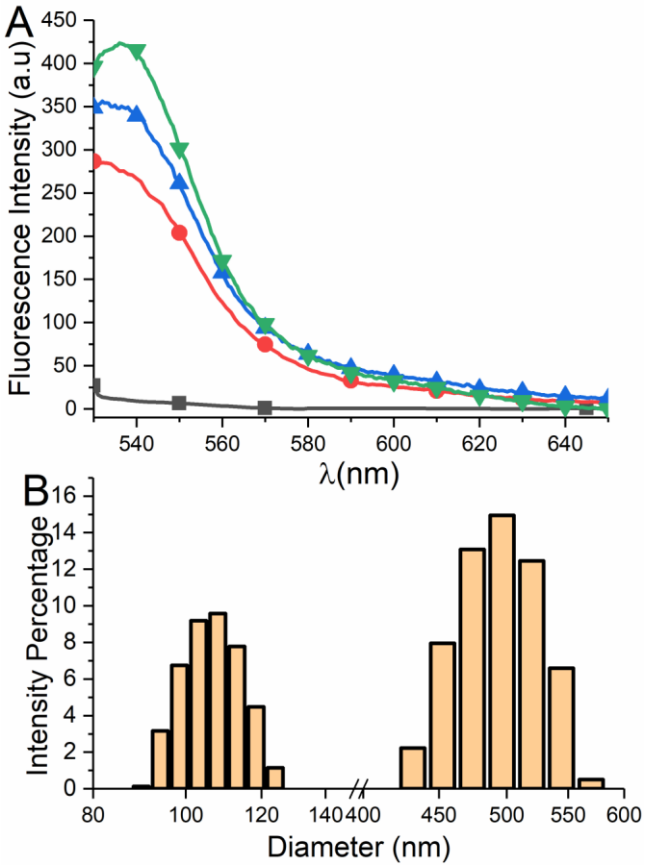

Figure 1. Characterization of p31-43 oligomers in solution by BODIPY fluorescence and Dynamic Light Scattering. **A)** Fluorescence emission spectra of p31-43 in presence of BODIPY at 1µM final concentration in presence of different peptide concentration solutions: (●) 10, (▲) 50 and (▼) 100µM peptide final solution. The buffer plus the probe was used as control (■). The excitation wavelength was 525 nm and the slits used were 5nm for the excitation and emission. Triplicates were performed for each condition **B)** Hydrodynamic diameter distribution of p31-43 obtained by Dynamic Light Scattering at 125µM concentration prepared in MilliQ water. The sample was previously centrifuged and filtered to eliminate particles and / or big aggregates and analyzed by triplicate.

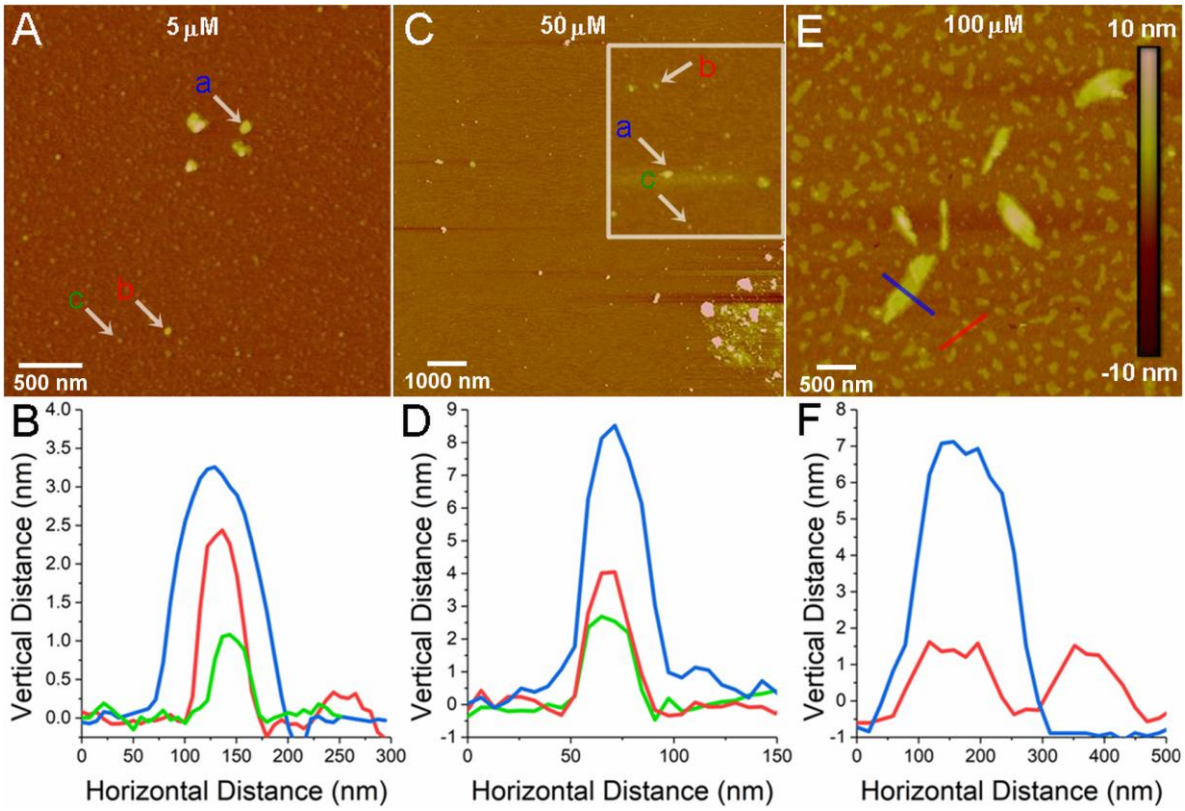

Figure 2. Morphological characterization of p31-43 oligomers
Gliadin p31-43 solutions at different concentrations in Milli Q water were deposited on mica surface and AFM images were obtained in tapping mode. **A)** 5μM p31-43 solution (3 x 3μm^2). **B)** Cross-section of the oligomers indicated in A. **C)** 50μM p31-43 solution (10 x 10μm^2). A zoom in the top left corner of the image shows different oligomeric species. **D)** Cross-section of the oligomers indicated in C: **E)** AFM image of 100μM peptide solution (5 x 5μm^2). **F)** Cross-section of the structures indicated in E. Color reference for cross-section images: (**a**) blue: higher oligomers, (**b**) red: intermediate oligomers and (**c**) green: smaller oligomers. The sample at each condition was analyzed by duplicate.

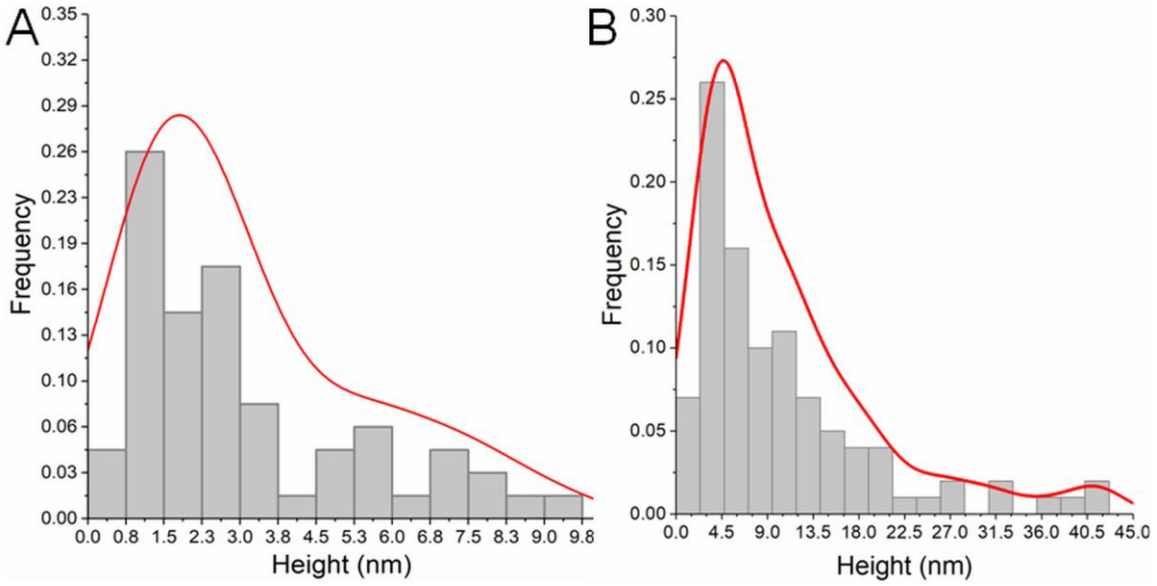

Figure 3. **Height distribution of the structures observed by AFM**. Analysis of the samples at A) 5 μM concentration (n= 50) and B) 50 μM concentration (n=100).

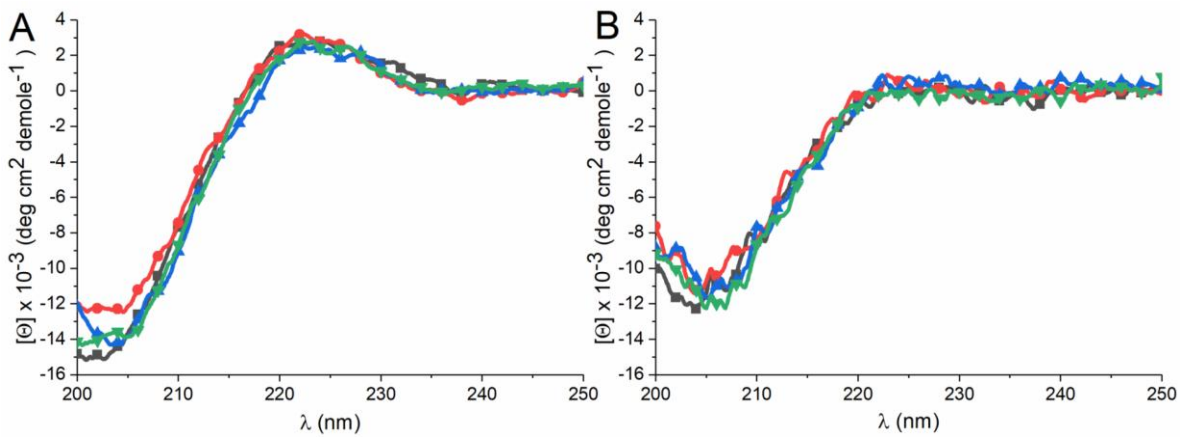

Figure 4. Circular Dichroism of p 31-43 in phosphate buffer at different pHs. Analysis at pH 3.0 (■), pH 5.0 (●), pH 7.4 (▲) and pH 8.0 (▼) **A)** at 4°C and **B)** at 37°C. The spectrum obtained at each condition represents and average of 5 spectra accumulation.

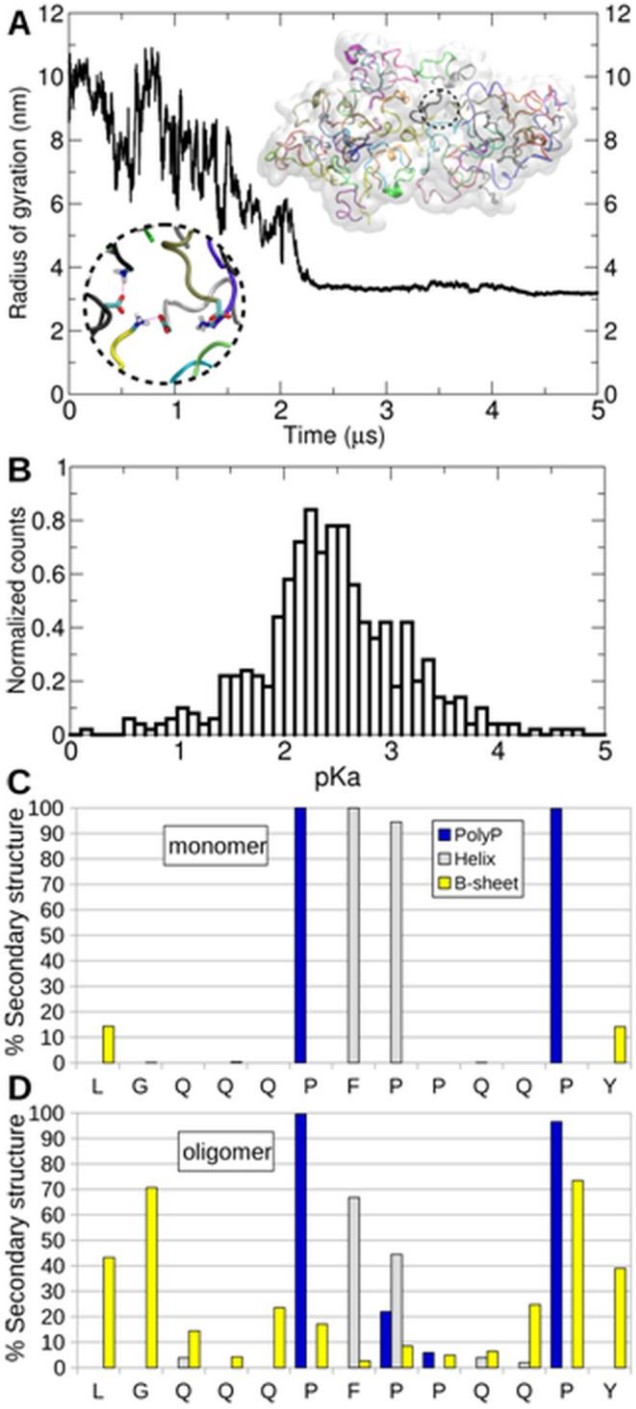

Figure 5. Coarse-grained Molecular Dynamics simulations of p31-43. **A)** The radius of gyration of 50 monomers of the peptide along the simulation. The marked decrease suggests that oligomerization happens spontaneously in absence of significant energetic barriers. In the final configuration (lower inset) the termini of the peptides form salt bridges that optimize electrostatics interactions (bottom inset). **B)** Normalized counts of pKa values assigned by PropKa of the carboxylate moieties of p31-43. Comparison between the average secondary structure of: **C)** an isolated monomer and **D)** the oligomer formed by 50 peptides. pKa values and secondary structure contents of the p31-43 oligomer were

averaged during the last 100 ns of simulation and over 50 replicas of the peptide contained inside the simulation box.

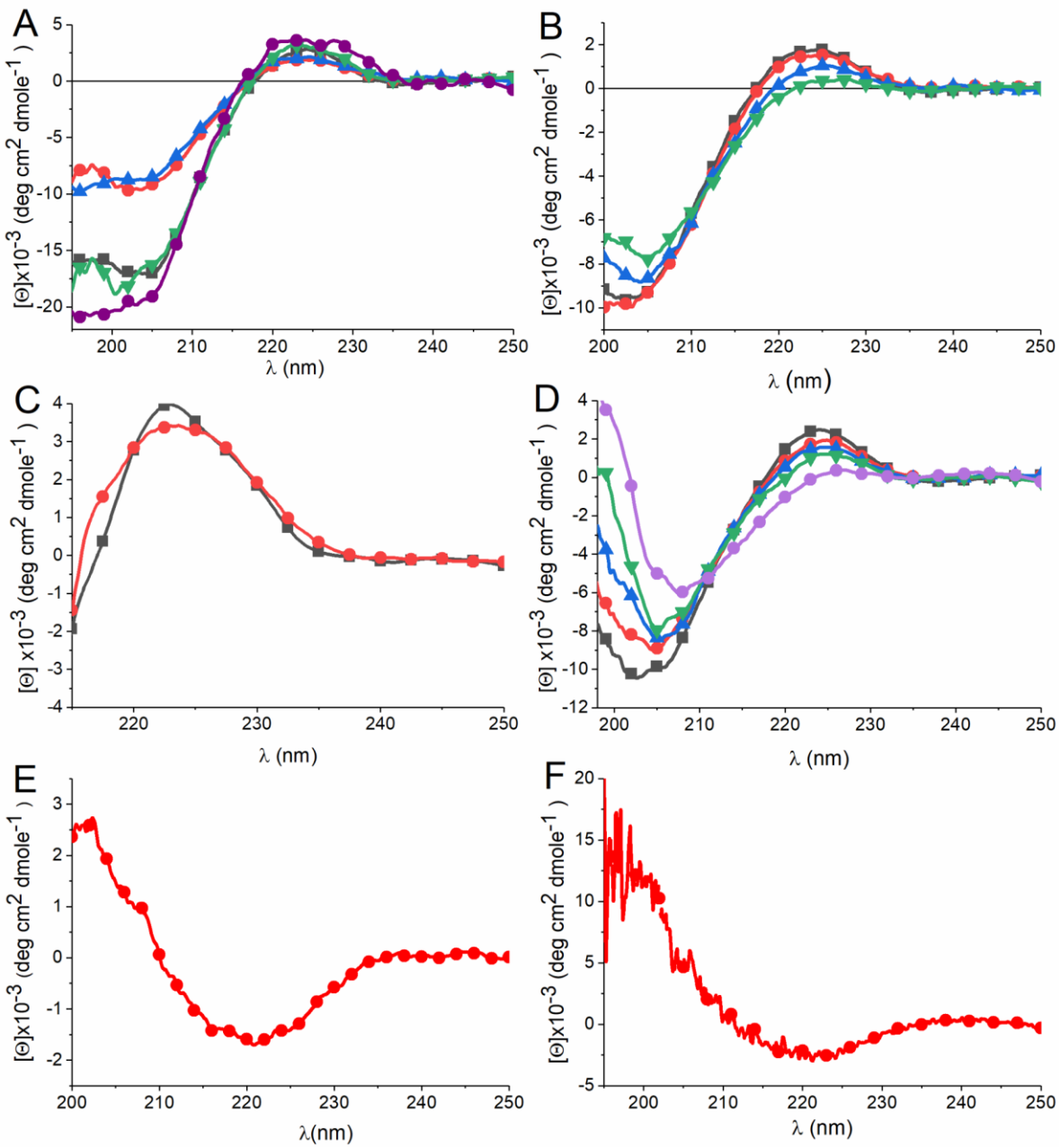

Figure 6. Structural analysis of p31-43 by Circular Dichroism shows PPII structure in equilibrium with β-sheet like structures. A) Spectra obtained at (●) 10μM (▼) 50μM, (■) 100μM, (▲) 200μM and (●) 500μM peptide solution at 4ºC. **B)** Spectra of a 200μM solution at (●) 4ºC, (■) 10ºC, (▲) 25ºC and (▼) 37ºC. **C)** Spectra obtained at (●) 50μM and (■) 200μM in 8M urea at 25°C. **D)** Spectra of a 200μM solution at difference concentrations of TFE: (■) 0%, (●) 10%, (▲) 20% and (▼) 30% and (●) 50% at 4°C. **E)** Difference spectra of 37°C and 4°C spectra presented in figure B). **F)** Difference spectra of 0% and 50% TFE spectra presented in figure D). The spectrum obtained at each condition represents an average of 5 spectra accumulation.

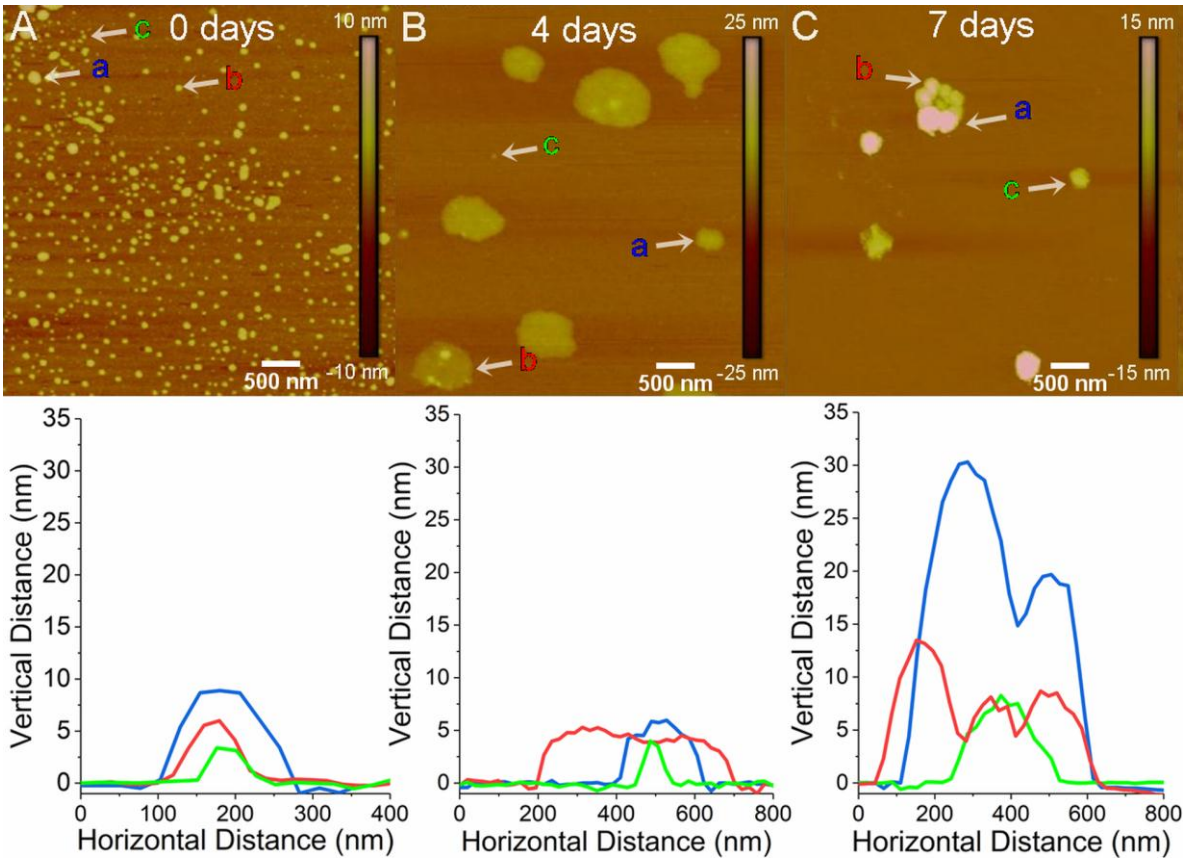

Figure 7: Time dependent morphological changes of p31-43 gliadin peptide at 10 µM. AFM images were obtained in tapping mode (5 x 5µm^2) by depositing the samples on the mica surface and drying by a nitrogen flux. The solutions were prepared in MilliQ water and incubated at 4°C at different time periods: **A)** freshly prepared sample (0 days) **B)** 4 days and **C)** 7 days. Below each AFM image it is presented the cross section of the structures detected. In blue (**a**) the highest, in red (**b**) the middle and in green (**c**) the smallest structures detected. The sample at each condition was analyzed by duplicate.

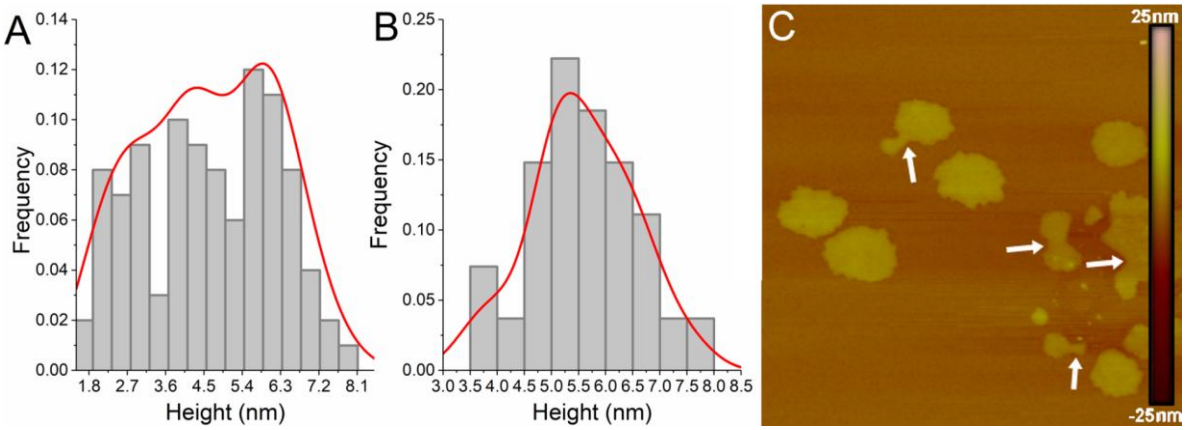

Figure 8 Characterization of the structures observed by AFM of the 10 µM solution of p31-43. In **A)** it is presented in the size of the structures showed in figure 5 A (freshly prepared solution, n=100), **B)** correspond to figure 5 B (4 days incubated solution, n=25). **C)** In this image it is shown by arrows the self-association of the different structures.

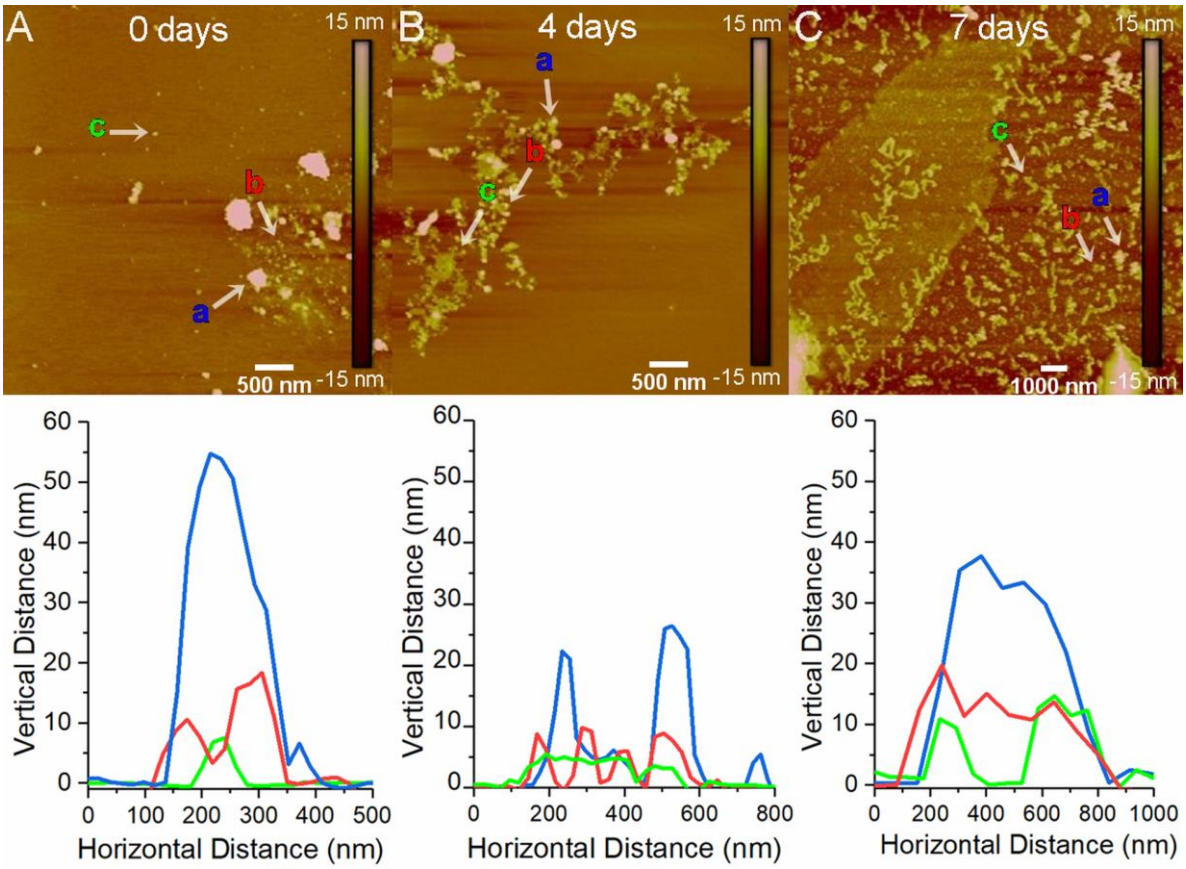

Figure 9: Time dependent morphological changes of p31-43 gliadin peptide at 50μM. AFM images were obtained in tapping mode by depositing the samples on mica surface and drying them by nitrogen flux. The solutions were prepared in MilliQ water and incubated at 4°C at different time periods: **A)** freshly prepared sample (0 days, 5 x 5μm^2) **B)** Sample at day 4 (5 x 5μm^2) and **C)** sample at day 7 (15 x 15μm^2). Below each AFM image the cross section of the structures detected is presented. Color reference: blue (**a**) higher oligomers, red (**b**) intermediate oligomers and green (**c**) smaller oligomers. The sample at each condition was analyzed by duplicate.

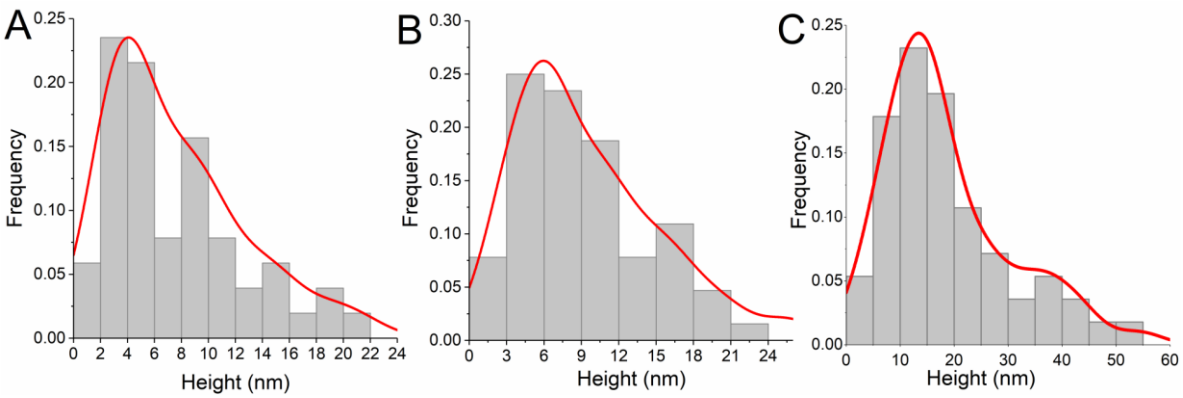

Figure 10. Height distribution of the 50 µM solution structures of p31-43 observed by AFM. In **A)** it is presented in the size of the structures showed in figure 6 A (freshly prepared solution, n=50), **B)** correspond to figure 6 B (4 days incubated solution, n=50) and **C)** to the figure 6C (7 days incubation, n=50).

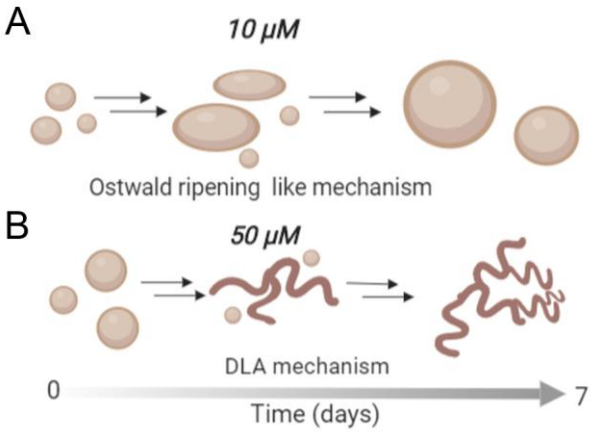

Figure 11. Scheme of proposed self-organization process of p31-43. **A)** At 10μm it is observed that at initial times the peptide self-assembly on small spherical oligomers that progress to form planar clusters at 4 days. At 7 days structures progress to form higher oligomers. This process may occur by a Ostwald ripening. **B)** At 50μM p31-43 generate at initial stages spherical oligomers of different heights. At 4 days interact forming linear arranges that progress to form fractal structures at 7 days. We propose that at this concentration the self-assembly process is govern by Diffusion Limited Aggregation (DLA)